LAWRENCE
LIVERMORE
NATIONAL
LABORATORY

UCRL-JRNL-220642

The Effect of Ring Substitution Position on the Structural Conformation of Mercaptobenzoic Acid Self-Assembled Monolayers on Au(111)

J. Lee, T. Willey, J. Nilsson, L. Terminello, J. De Yoreo, T. van Buuren

April 18, 2006

Langmuir

The Effect of Ring Substitution Position on the Structural Conformation of Mercaptobenzoic Acid Self-Assembled Monolayers on Au(111)

Jonathan R.I. Lee*, Trevor M. Willey, Joakim Nilsson,
Louis J. Terminello, James J. De Yoreo, Tony van Buuren

Lawrence Livermore National Laboratory,
Livermore, CA 94550

* lee204@llnl.gov

April 25, 2006

Abstract

Near edge X-ray absorption fine structure (NEXAFS)spectroscopy, photoemission spectroscopy (PES) and contact angle measurements have been used to examine the structure and bonding of self-assembled monolayers (SAMs) prepared on Au(111) from the positional isomers of mercaptobenzoic acid (MBA). The isomer of MBA and solvent chosen in SAM preparation has considerable bearing upon film morphology. Carbon K-edge NEXAFS measurements indicate that the monomers of 2-, 3- and 4-MBA have well-defined orientations within their respective SAMs. Monomers of 3- and 4-MBA assume an upright orientation on the Au substrates in monolayers prepared using an acetic acid in ethanol solvent. The aryl ring and carboxyl group of these molecules are tilted from the surface normal by a colatitudal angle of $\sim 30°$. Preparation of 4-MBA SAMs using pure ethanol solvent, a more traditional means of synthesis, had no appreciable effect upon the monomer orientation. Nonetheless, S(2p) PES measurements illustrate that it results in extensive bilayer formation via carboxyl group hydrogen-bonding between 4-MBA monomers. In 2-MBA monolayers prepared using acetic acid/ethanol solvent, the monomers adopt a more prostrate orientation on the Au substrates, in which the aryl ring and carboxyl group of the molecules are tilted $\sim 50°$ from the surface normal. This configuration is consistent with an interaction between both the mercaptan sulfur and carboxyl group of 2-MBA with the underlying substrate. S(2p) and C(1s) PES experiments provide supporting evidence for a bidentate interaction between 2-MBA and Au(111).

1 Introduction

The phenomenon of organothiol self-assembly on noble metal substrates is widely recognized as a facile and economical means of manipulating surface functionality [1]. Self-assembled monolayers (SAMs) of carboxyl terminated alkanethiols have attracted particular interest due to the diverse range of applications for which they are suited. Among their many uses, mercaptoalkanoic acid (MA) SAMs have been applied as biomimetic templates for inorganic crystal nucleation and growth [2, 3], surface tethers for

biologically active species [4, 5] and platforms for cell culture [6]. The SAMs have also been successfully employed as components in biosensors and immunosensors [7, 8, 9, 10] and show great promise in the development of molecular electronic devices [11]. In recent years, however, the isomers of mercaptobenzoic acid (MBA) have been identified as viable alternatives for preparing SAMs with carboxyl or carboxylate functionality [10, 13, 14, 15, 16, 17, 18, 19, 20, 21, 22, 23, 24]. In fact, MBA molecules offer two potential advantages over their MA analogues for engineering surfaces of technological value: firstly, the extended π-bonded system formed by the aryl and carboxyl groups facilitates charge transfer through the organic SAM overlayer [25]. In contrast, the alkyl chains in MA exhibit more insulating properties [26]. Secondly, MBAs form extremely thin SAMs (< 8 Å), which have been shown via STM [12] to contain a high degree of structural order. This is significant because SAMs of comparable thickness prepared from 'short chain' MAs contain substantial disorder [27].

Irrespective of the proposed merits in utilizing MBA for surface modification, it is of fundamental importance to characterize the morphology and bonding within the SAMs if one is to better understand their behavior and confirm their suitability for a given application. In particular, the orientation of the assembled molecules and their interaction with neighboring adsorbates and/or the underlying substrate can have a profound impact upon the physical and chemical properties of a SAM [1] and must be determined for the isomers of MBA to provide greater insight into their functionality and performance. Although previous studies have addressed specific aspects of the morphology [28, 29, 30], stability [31] and bonding [32] of MBA monolayers adsorbed on a variety of substrates, additional characterization is essential in order to provide a more comprehensive assignment of structure and composition. Furthermore, evidence reported for MBA isomer-dependent monolayer properties [32] indicates that direct comparison between the morphology and bonding of SAMs prepared from each isomer of MBA must represent a central component of any extended structural analysis.

An investigation of the effects of preparation method upon MBA SAM structure and composition is also of paramount importance. In the experiments reported to date, ethanolic solutions of MBA have frequently been used with the belief that idealized, well-ordered, SAMs would result. Recent studies [33, 34, 35, 36] indicate, however, that pure ethanol solvent is unsuited to the formation of ordered monolayer films of many carboxyl terminated organothiol monomers. MA monolayers prepared in pure ethanol solvent, a traditional means of MBA SAM synthesis, were found to contain a high degree of structural disorder [33, 34]. Meanwhile, the use of pure ethanol solvent induced bilayer formation in the synthesis of mercaptomethylterphenylcarboxylic acid (MMTA), a carboxyl terminated organothiol monomer containing a triphenyl moiety, films on Au substrates [33]. Well-ordered MA and MMTA monolayers were only produced upon addition of 5 to 10% acetic acid [33, 34, 35] (or 2% CF_3COOH [36]) by volume to the pure solvent.

In this manuscript, we present the systematic investigation of the structure and bonding in SAMs prepared on Au(111) substrates from the three isomers of MBA. A combination of near edge X-ray absorption fine structure (NEXAFS), photoemission spectroscopy (PES) and contact angle measurement was used for characterization of the monolayers. Fourier transform infrared (FT-IR) spectroscopy measurements were also conducted for control purposes. As the primary focus of this work, the morphology and bonding of MBA monolayers prepared in acetic acid/ethanol solution are addressed and directly compared. It is demonstrated that monolayers of 2-MBA prepared in this manner exhibit distinct conformational differences with respect to their 3- and 4-MBA analogues. Moreover, we illustrate that these differences are consistent with 2-MBA interacting with the underlying Au(111) substrate via both the mercaptan and carboxyl groups, while 3- and 4-MBA bond only through the mercaptan [32]. 4-MBA SAMs prepared from pure ethanol solvent are also characterized and directly compared with their acetic acid/ethanol equivalents. It is reported that the change in solvent composition has a considerable effect upon the morphology of the resulting SAMs.

2 Experimental

2.1 Reagents and Materials

All reagents were obtained from commercial sources and used as received. 2-Mercaptobenzoic acid (95%), 3-mercaptobenzoic acid (95%) and sodium hydroxide (98%) were purchased from Aldrich. 4-Mercaptobenzoic acid (97%) and glacial acetic acid (99.7%) were purchased from VWR. Ethanol (200 proof) was supplied by Aaper. Au(111) samples were prepared under high vacuum by the thermal evaporation of 5 nm Ti (99.99%, VWR) and then 100 nm of Au (99.99%, VWR) onto Si(100). All samples were hydrogen flame annealed immediately prior to use following well-established experimental protocols [37].

2.2 Sample Preparation

Solutions of each mercaptobenzoic acid were prepared according to the method reported by Arnold *et al.* [33] for carboxyl terminated alkanethiols, in which the organothiol is dissolved in 5% (by volume) acetic acid/ethanol to yield the required concentration (1-2 mM in this study). Freshly annealed Au(111) samples were then immersed in the MBA solutions for 24-36 hours to allow for SAM formation. After this period, the samples were removed, rinsed with pure 5% acetic acid/ethanol solvent, dried in a diffuse stream of high purity N_2(g) and immediately transferred to ultrahigh vacuum for NEXAFS/PES measurements or the sample chamber of an FT-IR spectrometer (Nicolet, 470). For the control measurements, 4-MBA SAMs were also prepared by replacing the acetic acid/ethanol mixture with pure ethanol as the organothiol solvent and rinse. All MBA SAM on Au(111) samples were generated under the same ambient conditions.

2.3 Instrumentation

X-ray absorption and X-ray photoemission spectra were recorded on VUV BL8.2 of the Stanford Synchrotron Radiation Laboratory (SSRL, SPEARIII) at the Stanford Linear Accelerator (SLAC). BL8.2 is served by a bending magnet and a spherical grating monochromator [38] and offers an energy resolution of $\sim$ 0.2 eV for NEXAFS experiments conducted at the carbon K-edge. The cross-section of the focussed beam was approximately 1 mm in diameter at the sample surface. NEXAFS spectra were recorded simultaneously in both total electron yield (TEY) and Auger electron yield (AEY) modes. The TEY signal was obtained by measuring the total current leaving the experimental sample as the X-ray energy was scanned across the absorption edge. The AEY signal was provided by measuring the intensity of the appropriate Auger electron during the course of each scan. The Auger electron intensity was recorded at a fixed kinetic energy and 200 eV pass energy using a PHI15-255G cylindrical mirror analyzer (CMA) and associated OEM electronics. All NEXAFS signals were normalized to the I_0 current, which was recorded for the incident X-ray beam via a Au grid located upstream of the experimental sample. To ensure minimal effect on the I_0 signal from, predominantly organic, contaminants absorbed on the surface of the grid, it was frequently coated with a fresh layer of evaporated Au. All NEXAFS measurements were conducted at base pressures $\leq$ 1x10^{-9} torr. The degree of linear polarization, P, in the incident beam was determined prior to each series of X-ray absorption experiments via carbon K-edge NEXAFS measurements of highly oriented pyrolytic graphite (HOPG). NEXAFS spectra were recorded at a series of angles of incidence between a freshly cleaved sample of HOPG and the X-ray beam. The axes through which the HOPG was rotated were carefully selected such that comparison of the C(1s) $\rightarrow \pi^*$ resonance (henceforth referred to as the 'π^* resonance/transition') intensity in the NEXAFS spectra yielded the relative magnitudes of ${E_p}^2$ and ${E_s}^2$, where E_p and E_s represent the electric field in-plane and perpendicular to the plane of incidence respectively. P was then calculated according to [39, 40]:

$$P = \frac{E_p^2}{E_s^2 + E_p^2} \quad (1)$$

The calculated polarization was 99% in the plane of the storage ring during the course of the experiments presented in this manuscript. For carbon NEXAFS measurements, the energy scale on BL8.2 was cali-

brated to the π^* resonance for HOPG, for which the energy was assigned to be 285.38 eV [41]. Care was taken to ensure that the effects of beam damage on the MBA SAM samples were minimized when conducting NEXAFS and PES measurements [42]. Each spectrum was recorded from a fresh region of the sample surface and beam exposure during data collection was limited to the timeframe required for good signal to noise statistics. For carbon K-edge NEXAFS, which was collected over a spectral range of 280-325 eV, this corresponded to $\sim$ 5 min per spectrum. In contrast, only $\sim$ 3 min was required for each PES spectrum.

All PES data was recorded using the PHI15-255G CMA, which was operated at a pass energy of 25 eV. C(1s) spectra were obtained at an incident photon energy of 400 eV; S(2p) spectra were obtained at incident photon energies of 280 and 400 eV. For the purposes of energy calibration, a PES spectrum of the Au 4f electrons was recorded immediately after each C(1s) and S(2p) measurement on the same region of the sample surface. The Au($4f_{7/2}$) photoelectron at 84.01$\pm$0.05 eV was then used to convert from kinetic energy to binding energy scales. FTIR spectra were collected in a reflecting grazing incidence geometry using a Nicolet 470 spectrometer equipped with an MCT detector. A background signal was obtained prior to each measurement using a freshly annealed Au(111) substrate. All contact angle measurements were conducted in a static sessile drop mode using a Krüss G10/DSA10 drop shape analysis system.

2.4 Analysis

NEXAFS yields a quantitative assignment of bond orientation through analysis of the polarization dependencies of various resonances. Hence, the technique can be used to determine the orientation of the aromatic ring and carboxyl group in the molecules that comprise the MBA SAMs. The intensity of a NEXAFS resonance is proportional to the dot product of the electric field vector in the X-ray beam and the transition dipole moment for the unoccupied orbital. For the MBA SAMs, Au(111) has three-fold azimuthal symmetry. The transition dipole moment can be modeled as a vector for the π^* orbital that extends throughout the aryl and carboxyl groups of MBA and lies perpendicular to the plane of the molecule. For resonances modeled by a vector transition dipole moment, the intensity, I_v, is expressed as [39, 40]

$$I_v(\theta,\alpha) \propto \frac{1}{3}P[1+\frac{1}{2}(3\cos^2\alpha-1)(3\cos^2\theta-1)] + \frac{1}{2}(1-P)\sin^2\alpha \quad (2)$$

where θ represents the angle between the incident radiation and the surface ($\leq 90^\circ$) and α represents the angle between the transition dipole moment vector, $\overrightarrow{M}$, and the surface normal. It is noted that there is a substantial separation in energy between the π^* resonances for the aryl and carboxyl carbon atoms due to the electron withdrawing effect of the oxygen atoms on the carboxyl carbon. As a consequence, these resonances are clearly resolved from one another in spectra collected on BL8.2. For the C-C and C-O σ^* orbitals and the Rydberg (R*) [43]/C-H σ^* resonances, the transition dipole moment is modeled by a plane, which is co-incident with the plane of the aryl ring in MBA. In this instance, the resonance intensity I_p is expressed as [39, 40]:

$$I_p(\theta,\gamma) \propto \frac{2}{3}P[1-\frac{1}{4}(3\cos^2\theta-1)(3\cos^2\gamma-1)] + \frac{1}{2}(1-P)(1+\cos^2\gamma) \quad (3)$$

where γ represents the angle between the surface normal and the normal to the plane of the transition dipole moment. To remove the proportionality, ratios are taken between spectra recorded at different angles of incidence. In order to simplify analysis, the intensities are left as functions of cosine squared. With $\Theta = \cos^2\theta$, $A = \cos^2\alpha$, $\Gamma = \cos^2\gamma$, the intensities from eqs 2 and 3 become:

$$\frac{I_v(\Theta_i,A)}{I_v(\Theta_j,A)} = \frac{P(3A-1)\Theta_i - A + 1}{P(3A-1)\Theta_j - A + 1} \quad (4)$$

and

$$\frac{I_p(\Theta_i,\Gamma)}{I_p(\Theta_j,\Gamma)} = \frac{P(3\Gamma-1)\Theta_i - \Gamma - 1}{P(3\Gamma-1)\Theta_j - \Gamma - 1} \quad (5)$$

respectively. These two equations are linear in Θ_i. A linear regression is obtained from all spectra acquired at Θ_i versus all spectra acquired at Θ_j, which allows α and γ to be solved as a function of the slopes or offsets. In principle, a high degree of precision, $< \pm 1°$, is possible from regression analysis on spectra recorded at multiple angles of incidence. Nevertheless, several additional sources of systematic error are omitted from this estimate and the predicted accuracy is actually between ±4-5°.

3 Results and Discussion

Figures 1(a) to (d) contain representative carbon K-edge NEXAFS spectra recorded for SAMs of MBA on Au(111) prepared according to the experimental protocols outlined previously. The spectra were collected for a series of angles between the plane of the sample surface and the axis of the X-ray beam ranging from normal (90°) to approaching grazing (20°) incidence. Angles of incidence below 20° were not measured due to constraints imposed by the relative dimensions of the sample and the X-ray beam cross-section. The upper panels of figures 1(a) to (d) display the raw NEXAFS spectra following normalization to the absorption edge step. The magnitude of the step was taken to be the difference between absorption signals recorded in the pre-edge (280 eV) and immediately post-NEXAFS (325 eV) regions for the scan of interest. To obtain the corresponding difference spectra presented in the lower panels of figures 1(a) to (d), the 20° scan was subtracted from the spectra collected at each of the other angles of incidence. Intense peaks in the difference spectra are indicative of polarization dependence in the orbital responsible for the NEXAFS resonance and, therefore, of well-defined bond/functional group orientation. Moreover, a preliminary assignment of this bond orientation can be inferred from inspection of the peak direction. For the experimental geometry employed in this study, intense peaks pointing downward in the difference spectra indicate that the transition dipole moment vector is oriented between the Au(111) surface normal and the magic angle ($\arcsin[(2/3)^{1/2}]$, $\sim 54.7°$, from the surface normal). Equally, peaks directed upward denote that the transition dipole moment vector is aligned more closely with the surface plane, oriented at least 54.7° from the surface normal.

Several pronounced NEXAFS resonances are observed in figures 1(a) to (d). The intense resonance at 285.3 eV is attributed to π^* transitions for the six carbon atoms contained within the aryl ring. It is noted that the FWHM of this resonance is greater than reported for the equivalent resonance in spectra of benzenethiol on Mo(110) [39] and that a shoulder is present at 285.6 eV. These features arise due to differences in the C(1s) orbital energies, which result from the variation in relative proximities of the aryl carbons to the electron-withdrawing oxygen atoms of the carboxyl group. The sharp resonance at 288.5 eV corresponds to the π^* transition for the carboxyl carbon. This spectral feature is convoluted with unresolved resonances at $\sim$ 287 eV and $\sim$ 288 eV that have been attributed to the C-S σ^* and C-H σ^*/R^* transitions [39]. The carboxyl π^* resonance is observed at a higher incident photon energy than the aryl carbon π^* resonances due to the strong inductive effect of the oxygen atoms on the carboxyl carbon. Two broad peaks are also visible at 294.2 and 303.0 eV. These features are assigned to C(1s) $\rightarrow$ C-C σ^* transitions [34, 39].

The carbon K-edge NEXAFS spectra of 2-, 3- and 4-MBA SAMs prepared from acetic acid/ethanol solvent (figures 1(a) to (c) respectively) all demonstrate strong polarization dependence in the aryl and carboxyl π^* transitions and, as a consequence, well-defined molecular orientation. In addition, comparison of the difference spectra indicates a significant contrast in the orientation of the 2-MBA molecules versus the 3- and 4-MBA within their respective monolayers. Both π^* resonances are more intense at grazing than normal beam incidence for 2-MBA and, therefore, the transition dipole moment vector of the π^* orbital is oriented within the 54.7° of the Au(111) surface normal. For 3- and 4-MBA, the π^* resonances are more intense at normal than grazing beam incidence, which signifies that the corresponding vectors are more closely aligned with the substrate surface. Since the π^* transition dipole moment vector is perpendicular to the plane containing the aryl and carboxyl groups, it is evident that the 3- and 4-MBA

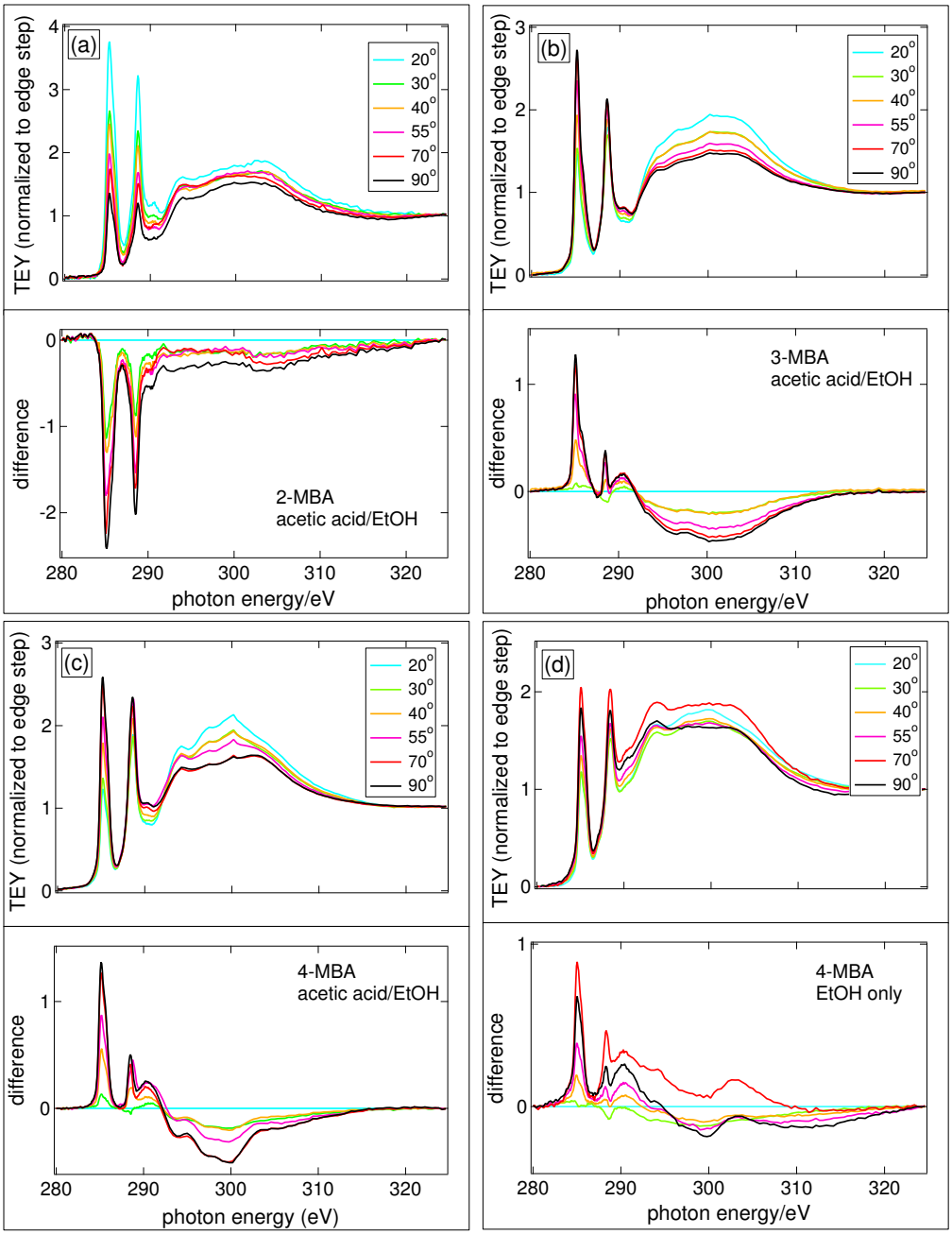

Figure 1: Normalized carbon K-edge NEXAFS spectra recorded in the TEY mode for **(a)** 2-MBA, **(b)** 3-MBA and **(c)** 4-MBA SAMs prepared on Au(111) from the acetic acid/EtOH solvent and **(d)** a 4-MBA SAM prepared on Au(111) from the EtOH only solvent

molecules adopt a more upright configuration than the 2-MBA (figure 2).

A more quantitative assignment of molecular orientation was achieved via regression analysis of the π^* resonance intensities for the aryl carbons (see Supplemental Information). Table 1 contains the tilt (colatitudal) angle obtained using this method for the plane of each MBA isomer with respect to the Au(111) surface normal. A regression analysis was also conducted for the carboxyl π^* resonance intensities. In this instance, modeling of the experimental spectra was essential in order to deconvolute the carboxyl π^* resonance intensities from C-S σ^* and C-H σ^*/R^* contributions at comparable energies. The peak fitting method employed for this purpose has been described in detail elsewhere [34]. The measured tilt angles were all within experimental error of those determined for the corresponding aryl π^* transitions, which one would expect for MBA monomers comprised of a coplanar aryl ring and carboxyl group.

The averaged tilt angles calculated for 3- and 4-MBA are within experimental error of one another and are in the range of 25-30° from the surface normal. As such, the 3- and 4-substituted monomers have an upright, but not entirely vertical, configuration (figures 2(b) and (c)). Given this assignment of molecular orientation, it is expected neither the 3- nor 4-MBA interact with the Au(111) surface through the carboxyl group, which would correlate

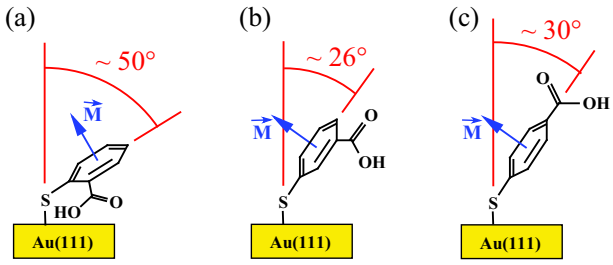

Figure 2: Schematic diagram indicating the molecular tilt angles for (a) 2-MBA, (b) 3-MBA and (c) 4-MBA in their respective SAMs on Au(111). The transition dipole moment vector for the extended π system of each molecule is included for clarity

with the findings of Wells *et al.* [32]. Within the experimental geometry utilized in this study, however, the possibility of a carboxyl-Au interaction for 3-MBA cannot be excluded purely from analysis of the NEXAFS. The spectra do not contain sufficient information regarding the degree to which the MBA molecules are rotated about the axis co-incident with the C-S σ-bond. Rotation about this axis could place the carboxyl group of 3-MBA in close enough proximity to interact with the underlying substrate.

It is interesting to note that there is a remarkable similarity in the polarization dependence of the aryl π^* resonance in NEXAFS spectra collected for 4-MBA SAMs prepared from pure ethanol (figure 1(d)) and acetic acid/ethanol solvent (figure 1(c)). Furthermore, the tilt angles obtained following each preparation method differ by $< 1.5°$. This result is somewhat surprising because it lies in direct contrast with the behavior of MA SAMs. When prepared from acetic acid/ethanol solvent, MA monolayers are known to be comprised of well-ordered surface arrays of defined orientation, whereas their pure ethanol equivalents contain substantial disorder [34]. The disparity between the behavior of these monolayers was attributed to disruption of the SAM structure by MA dimers formed at the substrate surface in pure ethanol solvent. Each dimer is formed by hydrogen-bonding between the carboxyl group of one MA molecule bound to the Au(111) surface and a second 'unbound' monomer. It has been reported that the formation of equivalent hydrogen-bonded dimers is less prevalent in 4-MBA SAMs prepared in the absence of acetic acid than for MAs [12, 28], which would provide an explanation in part for the similarity in orientation of 4-MBA molecules observed in this work. Even so, the resistance of the monolayers to disruption via dimerization implies that there are strong intermolecular interactions between neighboring adsorbates. Given that there is negligible hydrogen-bonding between the carboxyl groups of neighboring 4-MBA molecules bound to Au(111) [28], van der Waals interactions represent the most viable source of bonding between adsorbed surface monomers. Van der Waals dominated monolayer packing would also correlate with the formation of an ordered arrangement of 4-MBA molecules on Au(111), such has been

	tilt angle (°)	elemental sulfur (%)	bound thiolate (%)	unbound mercaptan (%)	contact angle (°)
2-MBA	49.6	5 ± 3	87 ± 3	7 ± 4	36.4
3-MBA	25.8	3 ± 3	71 ± 3	19 ± 3	20.8
4-MBA	29.6	2 ± 2	72 ± 4	17 ± 4	18.4
4-MBA (EtOH Only)	28.5	10 ± 3	54 ± 3	27 ± 3	-

Table 1: Colatitudal tilt angles and integrated S(2p) PES resonances for SAMs of each isomer of MBA on Au(111). The tilt angles have an accuracy of ± 4-5% and the contact angles have an accuracy of ± 2-3°.

observed by Schäfer *et al.* via STM [12].

It has been demonstrated [44, 45] that organothiol monomers with molecular structures comparable to 4-MBA exhibit well-defined monolayer arrangements and intermolecular packing. In particular, monomers dominated by a biphenyl moiety are known to adopt a herringbone-like arrangement on Au(111), in which monolayer packing is governed by σ(C-H)-π van der Waals interactions between neighboring adsorbates. Within these monolayers, the biphenyl based monomers adopt more upright than prostrate orientations on the underlying Au [46] and, importantly, exhibit closely comparable molecular tilt angles to 4-MBA. Molecular dynamics simulations conducted by Jung *et al.* [47] illustrate that molecules of benzyl mercaptan adsorbed on Au(111) in herringbone-like SAM arrangements would also have similar tilt angles to 4-MBA. Hence, it is probable that monolayers of 4-MBA adopt a herringbone-like packing scheme. Even so, alternative monolayer structures, such as those based upon π-π van der Waals interactions, cannot be excluded by analysis of the molecular tilt angle alone. It is important to state that comparison of the tilt angle with the STM images [12] reported for 4-MBA on Au(111) does not provide a more definitive assignment of the monolayer packing. Although the images display a periodic row structure, the closest approach between bright features is 8 Å. This distance is greater than the maximum separation that would allow for van der Waals interactions (based upon the van der Waals dimensions of a phenyl ring, 6.4 by 3.3 Å [48]) or carboxyl group hydrogen-bonding between neighboring monomers at tilt angles of $\sim 30°$.

The close similarity between tilt angles recorded for 3- and 4-MBA indicates that Van der Waals interactions could also be significant in the surface ordering of 3-MBA. In fact, an ordered monolayer structure based upon either σ(C-H)-π or π-π interactions would be consistent with the reported prevalence of hydrogen-bonding between adjacent 3-MBA monomers [32]. In the event of σ(C-H)-π based monolayer packing, hydrogen-bonding would be possible between the carboxyl groups of adjacent rows within a herringbone-like structure. For well-ordered SAMs dominated by π-π interactions, hydrogen-bonding would be possible between the carboxyl groups of neighboring 3-MBA monomers positioned with the aryl rings edge to edge (i.e. the hydrogen-bonding would occur in the orthogonal direction to the π-π interaction within the plane of the substrate).

An average tilt angle of 49.6° with respect to the surface normal was measured for 2-MBA monolayers prepared on Au(111). Hence, the plane of 2-MBA is angled $\geq 20°$ closer to the the Au(111) surface than the plane of either 3- or 4-MBA (figure 2(a)), which implies that the bonding interactions within SAMs of 2-MBA must differ substantially from those present in monolayers of the other isomers. While the 2-MBA adopts a slightly more prostrate than upright orientation, the $\sim 40°$ angle between the plane of the molecule and the underlying substrate precludes any interaction between the extended π-orbital and the Au(111) surface comparable with the bonding reported for isonicotinic acid on Ag sol [49]. Nevertheless, the carboxyl group is in close enough proximity to interact with the substrate surface with only minimal ($< 10°$) rotation about the axis of the C-S σ-bond. As such, the molecular orientation is consistent with the formation of a carboxyl-Au bond,

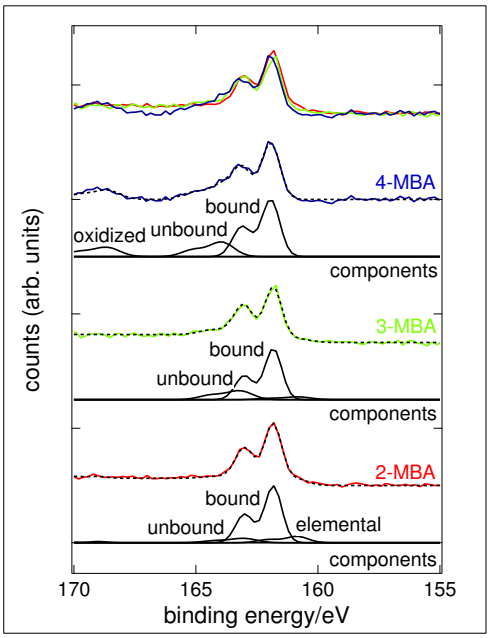

Figure 3: Sulfur S2p photoemission spectra for SAMs of each MBA isomer prepared on Au(111) from acetic acid/EtOH solvent

which has been proposed previously in FT-IR studies of 2-MBA monolayers [32]. Although the presence of a carboxyl-Au bond accounts for a difference in tilt angle of 2-MBA with respect to 3- and 4-MBA, it remains unclear whether interactions between neighboring molecules are also important in controlling the specific orientation adopted by 2-MBA. It is evident that minimal, if any, intermolecular hydrogen-bonding can occur within the monolayers due to the carboxyl-Au bond formation. At a molecular tilt angle of $\sim 50°$, however, the possibility of σ(C-H)-π or π-π van der Waals interactions cannot be excluded.

Additional characterization of the MBA monolayers was conducted using PES. Figure 3 contains representative S(2p) PES spectra recorded for monolayers of each MBA isomer prepared from the acetic acid/ethanol solvent. The accompanying best fit model spectra are comprised of four separate S(2p) resonances, each of which corresponds to a specific sulfur environment near the substrate surface. All of the resonances are spin-orbit split into doublets with a branching ratio of $\sim$ 2:1 and an energy separation of $\sim$ 1.2 eV. The S $2p_{3/2}$ (S $2p_{1/2}$) resonance near 161.9 eV (163.1 eV) arises from Au-bound thiolate [50] and lies between resonances at 160.8 eV (162.0 eV) and 163.2 eV (164.4 eV) which correspond to 'elemental' sulfur and the mercaptan sulfur of the 'unbound' monomers respectively. The final resonance, observed around 167.1 eV (168.3 eV), results from oxidized sulfur. This resonance was used as a preliminary diagnostic of sample preparation. SAMs containing $>$ 10% contribution from oxidized sulfur were assumed to have degraded via exposure to atmospheric oxygen and deemed unsuitable for study with NEXAFS. Table 1 contains the integrated relative intensities of the S(2p) PES resonances for each MBA SAM. All intensities are corrected for photoelectron attenuation by the SAM according to the methodology of Lamont *et al.* [51] and monolayer thicknesses were calculated from the appropriate tilt angles.

It is clear from inspection of the S(2p) PES spectra that monomers bound to the Au(111) substrate via the sulfur atom predominate for all isomers of MBA. There is a substantial difference, however, in the proportion of the unbound molecules contained within the SAMs. Monolayers of 2-MBA contain $\sim$ 7% of the unbound mercaptan, which is comparable with SAMs prepared from acetic acid/ethanol solutions of MAs [34], whereas SAMs of 3- and 4-MBA incorporate closer to 20%. These concentrations are consistent with the molecular orientations obtained from the NEXAFS. At a tilt angle of 29.6°, carboxyl groups of surface bound 4-MBA are directed away from the underlying substrate and, therefore, are accessible for hydrogen-bonding and dimerization with unbound molecules. A comparable situation can be envisioned for adsorbed monomers of 3-MBA, provided there is minimal rotation about the C-S σ-bond forcing the carboxyl group away from the monolayer surface. In contrast, the carboxyl group of adsorbed 2-MBA is directed towards the Au(111) surface and would be inaccessible for hydrogen-bonding interactions, even in the absence of a carboxyl-Au bond.

There exists the possibility that a component of the

unbound mercaptan signal for 3- and 4-MBA arises from monomers bound to the Au(111) substrate via the carboxyl group. Analysis of the corresponding C(1s) PES spectra (figure 4), however, illustrates that these interactions are extremely limited. Two distinct peaks are observed in the spectra of each MBA isomer: the first, an intense and asymmetric peak at a binding energy of 283.7 eV, is attributed to photoelectrons emitted from carbon atoms within the aryl ring and shows minimal variation from spectrum to spectrum. The second, a less intense resonance observed at higher binding energy, corresponds to photoelectrons from the carboxyl carbon. Both the difference in C(1s) binding energy between the aryl and carboxyl carbons and the asymmetry of the aryl carbon peak arise due to the inductive effects of the electron-withdrawing oxygen atoms discussed in reference to the NEXAFS π-resonances. Within experimental error, the carboxyl carbon peaks for the 3- and 4-MBA SAMs exhibit identical binding energies (288.0 eV) and FWHM (1.3 eV), which indicates that the carboxyl carbons are in similar environments. In comparison, the carboxyl carbon peak for the 2-MBA monolayer is observed at a lower binding energy, 287.6 eV, than for SAMs of 3- and 4-MBA, has a reduced intensity and is broadened to a FWHM of 1.8 eV.

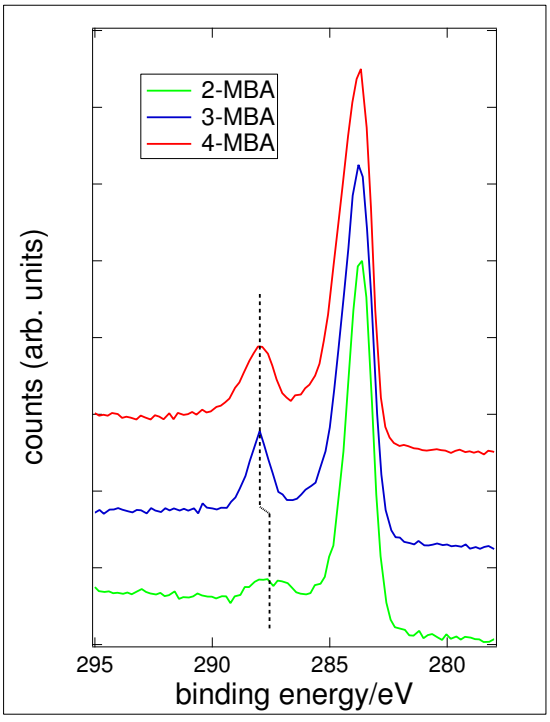

Figure 4: Carbon 1s photoemission spectra for SAMs of each MBA isomer prepared on Au(111)

The 0.4 eV shift in binding energy is attributed to a reduction in the inductive effect of the oxygen atoms on the carboxyl carbon due to the interaction between the carboxyl group and the Au(111) substrate. Therefore, if a significant proportion of 3- and 4-MBA monomers were bound to the substrate via the carboxyl group, it would be expected that the C(1s) PES spectra of their SAMs would contain a second carboxyl carbon peak around 287.6 eV comparable with the resonance observed for 2-MBA. Since this additional peak is not in evidence, the majority of unbound mercaptan within the 3- and 4-MBA SAMs must be contained in hydrogen-bound surface dimers. It is also apparent that 3-MBA does not bond to the substrate via both the mercaptan sulfur and carboxyl group simultaneously. In the absence of carboxyl-Au interactions within monolayers of 3- and 4-MBA, the carboxyl carbons must reside further from the underlying substrate and closer to the SAM surface than the carboxyl carbons within monolayers of 2-MBA. By extension, there will be greater inelastic scattering of the photoelectrons emitted by the carboxyl carbons of 2-MBA because they are buried deeper within the SAM. An increase in attenuation by the monolayer correlates with the observed reduction in intensity of the carboxyl carbon resonance for 2-MBA relative to 3- and 4-MBA. It is proposed that the accompanying increase in FWHM of this peak arises due to slight variations in the carboxyl-Au interaction within the 2-MBA monolayers.

The C(1s) PES spectra presented in figure 4 are similar to those described in the literature for SAMs prepared from pure ethanol solution [32]. In addition, the FT-IR spectra recorded for samples prepared from acetic acid/ethanol solution (see Supplemental Information) are also comparable to those reported for MBA monolayers assembled in ethanol only. De-

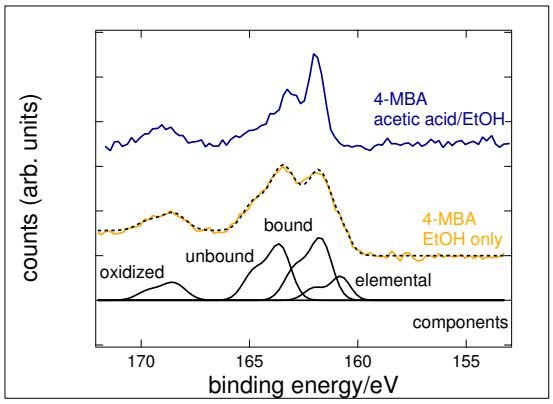

Figure 5: Sulfur 2p photoemission spectra for a 4-MBA SAM prepared on Au(111) from pure ethanol solvent. A spectrum for a 4-MBA SAM prepared in acetic acid/ethanol solvent is included for comparison.

spite these similarities, S(2p) PES measurements for 4-MBA SAMs prepared in pure ethanol indicate that the choice of solvent has an important bearing on the monolayer composition. A representative S(2p) PES spectrum for these monolayers and the accompanying best fit model are displayed in figure 5. The corresponding integrated relative intensities for the individual resonances that comprise this spectrum are included in table 1. In relation to 4-MBA SAMs prepared in the presence of acetic acid, the contribution to the total signal from bound monomers decreases by $\sim$ 20% and there is a 10% increase in the proportion of unbound molecules. Hence, the acetic acid acts to inhibit the formation of dimers between surface bound and unbound molecules, although with less efficiency than has been reported for MA SAMs [34]. It is noteworthy that the relative surface concentration ($>$ 25%) of unbound 4-MBA in SAMs prepared from pure ethanol solvent would account for the proportion of carboxyl group hydrogen-bonding indicated by FT-IR spectroscopy measurements of the monolayers [32]. Although this does not necessarily exclude the possibility of dimerization between adjacent, surface-bound, monomers via hydrogen-bonding, it demonstrates that any such interactions are limited at best.

Static contact angles of water recorded for SAMs prepared from each MBA isomer using the acetic acid/ethanol solvent are presented in table 1. Monolayers of 3- and 4-MBA on Au(111) exhibit static contact angles of $\theta_a \sim 20°$, which are within the range corresponding to hydrophilic surfaces. The hydrophilic behavior of each SAM denotes that the highly polar carboxyl groups of 3- and 4-MBA monomers must be readily accessible for interaction with the water molecules. A more hydrophobic surface would be anticipated if the carboxyl groups were buried within the SAMs and only the aryl or mercaptan groups were exposed instead. The hydrophilic nature of the 3- and 4-MBA monolayer surfaces correlates with the associated XPS and NEXAFS data: it has been established that the majority of carboxyl groups are located at the uppermost surface of the 4-MBA monolayers and must, therefore, comprise at least part of the interface formed with the water droplet. The close similarity in contact angle between SAMs of 3- and 4-MBA indicates that the carboxyl groups must also reside near the surface in monolayers of 3-MBA. As a result, it illustrates that there is insufficient rotation of 3-MBA about the C-S σ-bond to allow any carboxyl-Au interaction.

A static contact angle of $\theta_a \sim 36°$ was obtained for monolayers of 2-MBA, which indicates that their surfaces have a degree of hydrophilic character. The affinity between the 2-MBA SAMs and water could arise due to the presence of structural disorder within the organic layer. In a well-ordered structure, the surface-bound carboxyl groups would be buried within the monolayer, thereby largely preventing interaction with water. Aryl groups would predominate at the sample surface and the monolayer would be expected to display hydrophobic behavior. In more disordered structures, however, water could penetrate into the monolayer to reach the carboxyl groups and this would lead to increased hydrophilic character. As a basis for this interpretation, it is assumed that the carboxyl and water are too far apart to experience strong dipole-dipole interactions when separated by the thickness of the monolayer. Long range dipole-dipole interactions could exist between the carboxyl groups and water, but comparison with

the literature demonstrates that they are extremely unlikely to bring about contact angles on the order of $\sim 36°$. As an example, Bain *et al.* [52] report that SAMs prepared from methyl ester terminated alkanethiols are more hydrophobic (advancing contact angle of 67° with water) than SAMs of 2-MBA, even though their carbonyl moiety is much closer to the monolayer surface.

4 Conclusions

NEXAFS and PES studies indicate that the specific isomer used in MBA SAM preparation has a considerable impact upon the conformation and bonding of the resultant monolayers. It is also determined that the choice of solvent employed in synthesis has significant influence over the structure and composition of the MBA films. As such, selection of the appropriate isomer and preparation conditions are essential in surface functionalization with MBA for specific technological applications.

The use of an acetic acid/ethanol solvent in SAM formation produces monolayers of 2-, 3- or 4-MBA with well-defined monomer orientation. Carbon K-edge NEXAFS measurements illustrate that the monomers of 3- and 4-MBA adopt an upright orientation, in which the aryl ring and carboxyl group of the molecules are tilted by $\sim 30°$ with respect to the Au(111) surface normal. In contrast, the monomers of 2-MBA assume a more prostrate orientation on the substrate, with colatitudal tilt angles of closer to $\sim 50°$ for the aryl ring and carboxyl group. In this configuration, the monomers of 2-MBA can interact with the underlying Au via both the mercaptan sulfur and the carboxyl group simultaneously, as has been proposed from a combination of FT-IR and X-ray photoelectron spectroscopy measurements [32]. C(1s) and S(2p) PES experiments provide supporting evidence of concurrent Au-S and Au-carboxyl bonding for the adsorbed monomers of 2-MBA. Meanwhile, the PES measurements indicate that 3- and 4-MBA bond to the substrate surface through only the mercaptan sulfur. As a consequence, the carboxyl groups of 3- and 4-MBA are more accessible than those of 2-MBA for interaction with species present at the monolayer surface. This is reflected in the formation of a higher proportion of hydrogen-bonded surface dimers in SAMs of 3- and 4-MBA than in SAMs of 2-MBA. It is also illustrated via the contact angles with water measured for the MBA monolayers. 3- and 4-MBA monolayers prepared in the acetic acid/EtOH solvent exhibit greater hydrophilic character than their 2-MBA counterparts.

S(2p) PES measurements demonstrate that SAMs of 4-MBA prepared in pure ethanol solvent contain a substantially higher proportion of surface dimers than those synthesized in the presence of acetic acid. Hence, the use of the acetic acid/ethanol solvent serves to inhibit carboxyl group hydrogen-bonding between MBA monomers. Nonetheless, carbon K-edge NEXAFS experiments indicate that the extensive dimerization of 4-MBA monomers in pure ethanol solvent has minimal impact upon their orientation. The calculated tilt angles of the 4-MBA monomers are equivalent, to within experimental error, for the two solvents. As a result, it is proposed that there are strong van der Waals interactions between neighboring adsorbates.

5 Acknowledgements

This work was supported by the Division of Chemical Sciences, Office of Basic Energy Science, and performed under the auspices of the U.S. DoE by LLNL under Contract W-7405-ENG-48. Portions of this research were carried out at the Stanford Synchrotron Radiation Laboratory, a national user facility operated by Stanford University on behalf of the U.S. Department of Energy, Office of Basic Energy Sciences. The authors would like to thank the SSRL staff, particularly Dan Brehmer and Curtis Troxel, for their assistance during the course of these experiments.

References

[1] Ulman, A. *Chem. Rev.* **1996**, *96*, 1533

[2] Aizenberg, J.; Black, A.J.; Whitesides, G.M. *Nature* **1998**, *394*, 868

[3] Han, Y.-J.; Aizenberg, J. *Angew. Chem. Int. Ed.* **2003**, *42*, 3668

[4] Patel, N.; Davies, M.C.; Hartshorne, M.; Heaton, R.J.; Roberts, C.J.; Tendler, S.J.; Williams, P.M. *Langmuir* **1997**, *13*, 6485

[5] Patel, N.; Davies, M.C.; Heaton, R.J.; Roberts, C.J.; Tendler, S.J.; Williams, P.M. *Appl. Phys. A* **1998**, *66*, S569

[6] Scotchford, C.A.; Cooper, E.; Leggett, G.A.; Downes, S. *J. Biomed. Mater. Res.* **1998**, *41*, 431

[7] Disley, D.M.; Cullen, D.C.; You, H.X.; Lowe, C.R. *Biosens. Bioelectron.* **1998**, *13*, 1213

[8] Kerman, K.; Ozkan, D.; Kara, P.; Meric, B.; Gooding, J.J.; Ozsoz, M. *Analytica Chim. Acta* **2002**, *462*, 39

[9] Ozkan, D.; Erdem, A.; Kara, P.; Kerman, K.; Gooding, J.J.; Nielsen, P.E.; Ozsoz, M. *Electrochem. Comm.* **2002**, *4*, 796

[10] Vaughan, R.D.; O'Sullivan, C.K.; Guilbault, G.G. *Fresnius J. Anal. Chem.* **1999**, *364*, 54.

[11] Calvente, J.J.; López-Pérez, G.; Ramirez, P.; Fernndez, H.; Zon, M.A.; Mulder, W.H.; Andreu, R. *J. Am. Chem. Soc.* **2005**, *127*, 6476.

[12] Schäfer, A.; Seidel, C.; Chi, L.; Fuchs, H. *Adv. Mater.* **1998**, *10*, 839.

[13] Lu, C.; Wei, F.; Wu, N.; Huang, L.; Zhao, X.; Jiao, X.; Luo, C.; Cao, W. *Langmuir* **2004**, *20*, 974.

[14] Orendorff, C.J.; Gole, A.; Sau, T.K.; Murphy, C.J. *Anal. Chem.* **2005**, *77*, 3261.

[15] Matsui, H.; Gologan, B.; Pan, S.; Douberly Jr., G.E. *Eur. Phys. J. D* **2001**, *16*, 403.

[16] Nishino, T.; Ito, T.; Umezawa, Y. *Anal. Chem.* **1991**, *22*, 811

[17] Vaughan, R.D.; O'Sullivan, C.K.; Guilbault, G.G.; *Enzyme Microbial Technol.* **2001**, *29*, 635.

[18] Vaughan, R.D.; Carter, R.M.; O'Sullivan, C.K.; Guilbault, G.G. *Anal. Lett.* **2003**, *36*, 731.

[19] Park, I.-S.; Kim, D.-K.; Adanyi, N.; Varadi, M.; Kim, N. *Biosensors Bioelectronics* **2004**, *19*, 667

[20] Pinnaduwage, L.A.; Hawk, J.E.; Boiadjiev, V.; Yi, D.; Thundat, T. *Langmuir* **2003**, *19*, 7841.

[21] Pinnaduwage, L.A.; Boiadjiev, V.; Hawk, J.E.; Thundat, T. *Appl. Phys. Lett.* **2003**, *83*, 1471.

[22] Talley, C.E.; Jusinski, L.; Hollars, C.W.; Lane, S.M.; Huser, T. *Anal. Chem.* **2004**, *76*, 7064.

[23] Zangmeister, C.D.; van Zee, R.D. *Langmuir* **2003**, *19*, 8065.

[24] Volcke, C.; Simonis, P.; Durant, F.; Thiry, P.A.; Lambin, P.; Culot, C.; Humbert, C. *Chem. Eur. J.* **2005**, *11*, 4185.

[25] Creager, S.; Yu, C.J.; Bamdad, C.; O'Connor, S.; MacLean, T.; Lam, E.; Chong, Y.; Olsen, G.T.; Luo, J.; Gozin, M.; Kayyem, J.F. *J. Am. Chem. Soc.* **1999**, *121*, 1059.

[26] Bumm, L.A.; Arnold, J.J.; Cygan, M.T.; Dunbar, T.D.; Burgin, T.P.; Jones II, L.; Allara, D.L.; Tour, J.M.; Weiss, P.S. *Science* **1996**, *271*, 1075.

[27] Porter, M.D.; Bright, T.B.; Allara, D.L.; Chidsey, C.E.D. *J. Am. Chem. Soc.* **1987**, *109*, 3559.

[28] Creager, S.E.; Steiger, C.M. *Langmuir* **1995**, *11*, 1852.

[29] Michota, A.; Bukowska, J. *J. Raman Spectros.* **2003**, *34*, 21.

[30] Lee, S.B.; Kim, K.; Kim, M.S. *J. Raman Spectrosc.* **1991**, *22*, 811.

[31] Arihara, K.; Ariga, T.; Takashima, N.; Arihara, K.; Okajima, T.; Kitamura, F.; Tokuda, K.; Ohsaka, T. *Phys. Chem. Chem. Phys.* **2003**, *5*, 3758.

[32] Wells, M.; Dermody, D.L.; Yang, H.C.; Kim, T.; Crooks, R.M.; Ricco, A.J. *Langmuir* **1996**, *12*, 1989

[33] Arnold, R.; Azzam, W.; Terfort, A.; Wöll, C. *Langmuir* **2002**, *18*, 3980.

[34] Willey, T.M.; Vance, A.L.; van Buuren, T.; Bostedt, C.; Nelson, A.J.; Terminello, L.J.; Fadley, C.S. *Langmuir* **2004**, *20*, 2746.

[35] Dannenberger, O.; Weiss, K.; Himmel, H.J.; Jager, B.; Buck, M.; Wöll, C. *Thin Solid Films* **1997**, *307*, 183.

[36] Wang, H.; Chen, S.; Li, L.; Jiang, S. *Langmuir* **2005**, *21*, 2633

[37] Hydrogen flame annealing follows the method described by Molecular Imaging, Inc. in http://www.molec.com/anneal.html (accessed Aug 2005).

[38] Tirsell, G.K.; Karpenko, V.P. *Nucl. Instrum. Methods* **1990**, *A291*, 511.

[39] Stöhr, J.; Outka, D.A. *Phys. Rev. B* **1987**, *36*, 7891.

[40] Stöhr, J. *NEXAFS Spectroscopy*; Springer-Verlag, 1992.

[41] Batson, P.E. *Phys. Rev. B* **1993**, *48*, 2608.

[42] Zharnikov, M.; Grunze, M. *J. Vac. Sci. Technol. B* **2002**, *20*, 1793.

[43] Bagus, P.S.; Weiss, K.; Schertel, A.; Wöll, C.; Braun, W.; Hellwig, C.; Jung, C. *Chem. Phys. Lett.* **1996**, *248*, 129.

[44] Azzam, W.; Cyganik, P.; Witte, G.; Buck, M.; Wöll, C. *Langmuir* **2003**, *19*, 8262.

[45] Cyganik, P.; Buck, M.; Azzam, W.; Wöll, C. *J. Phys. Chem. B* **2004**, *108*, 4989.

[46] Rong, H.-T.; Frey, S.; Yang, Y.-J.; Zharnikov, M.; Buck, M.; Wühn, M.; Wöll, C.; Helmchen, G. *Langmuir* **2001**, *17*, 1582.

[47] Jung, H.H.; Won, Y.D.; Shin, S.; Kim, K. *Langmuir* **1999**, *15*, 1147.

[48] Fuxen, C.; Azzam, W.; Arnold, R.; Terfort, A.; Witte, G.; Wöll, C. *Langmuir* **2001**, *17*, 3689.

[49] Chattopadhyay, S.; Brahama, S.K. *Spectrochim. Acta, Part A* **1993**, *49*, 589.

[50] Castner, D.G.; Hinds, K.; Grainger, D.W. *Langmuir* **1996**, *12*, 5083

[51] Lamont, C.L.A.; Wilkes, J. *Langmuir* **1999**, *15*, 2037.

[52] Bain, C.D.; Troughton, E.B.; Tao, Y.-T.; Evall, J.; Whitesides, G.M., Nuzzo, R.G. *J. Am. Chem. Soc.* **1989**, *111*, 321.

This work was performed under the auspices of the U. S. Department of Energy by University of California, Lawrence Livermore National Laboratory under contract W-7405-Eng-48.